Structural Analysis of Silica-Supported Tungstates

Cristina Martín,[†] Pilar Malet,[‡] Gabriel Solana,[†] and Vicente Rives*,[†]

Departamento de Química Inorgánica, Universidad de Salamanca, Salamanca, Spain, and Departamento de Química Inorgánica-Instituto de Ciencia de Materiales, Universidad de Sevilla-C.S.I.C., P.O. Box 553, 41071 Sevilla, Spain

Received: January 2, 1998

The structure, surface acidity, and reducibility of WO_3/SiO_2 systems, obtained by impregnation of the silica support with aqueous paratungstate solutions, are described. The effect of tungsten loading and calcination temperature on the nature and physicochemical properties of tungsten-containing phases has been studied by FT-IR, Raman and W−L_3 XAS spectroscopies, X-ray diffraction, temperature-programmed reduction, and FT-IR monitoring of pyridine adsorption for surface acidity. Results obtained show that, due to a reaction between the tungstate and the support, calcination up to 723 K leads to formation of a Si−O−W crystalline species where tungsten is forming Keggin-type units similar to those found in dodecatungstosilicates. As the calcination temperature is raised, these species decompose leading to crystalline WO_3, due to the low dispersing ability of silica. Thermal stability of this Si−O−W species is higher than that of commercial dodecatugstosilicic acid, although it slightly decreases as the tungsten content decreases. Si−O−W species possess large surface acidity, with both Lewis and Brönsted acid sites, and they are more easily reduced than crystalline WO_3.

Introduction

Catalytic systems containing tungsten oxide have been described in the literature.[1−7] When preparing these systems, the effect on the catalytic performance of variables such as the preparation method, the nature of the support, and the concentration of the supported phases have been studied. Silica and alumina are the most common supports, probably because they are nearly inert supports, with a high specific surface area and mechanical strength. The WO_3/SiO_2 system has been applied in many cases for several catalytic reactions,[6,8−14] and the active phase has been usually described as a combination of surface species, namely distorted octahedral tungstates and crystalline WO_3; however, the precise nature of these tungstates is far to be completely understood and depends on the preparation method. Wachs et al.[15] have reported the preparation of WO_3/SiO_2 catalysts by impregnation of silica with aqueous solutions containing ammonium metatungstate or pentane solutions of $W(\eta^3\text{-}C_3H_5)_4$. These authors report formation of crystalline WO_3 in the first case after calcination of the precursor at 773 K, while this species was absent in the second case and, instead, Raman spectroscopy put into evidence formation of polytungstate clusters, $W_{12}O_{42}^{12-}$. In some cases, formation of heteropolyacids has been also described, and these represent a series of solids very interesting for heterogeneous acid and redox reactions.[16] In this paper, we report on tungsta/silica samples prepared by impregnation, containing different tungsten loadings and submitted to different calcination temperatures. The nature and properties of the species formed have been studied by FT-IR, Raman and W−L_3 XAS spectroscopies, X-ray diffraction, temperature-programmed reduction, and FT-IR monitoring of pyridine adsorption for surface acidity.

* Corresponding author. Fax +34 23 29 45 74; e-mail vrives@gugu.usal.es.
[†] Universidad de Salamanca.
[‡] Universidad de Sevilla.

Experimental Section

Sample Preparation. Samples were prepared by impregnation of silica from Degussa (specific surface area ca. 200 $m^2\ g^{-1}$) with aqueous solutions of ammonium paratungstate (Fluka, Buchs, Switzerland), using 10 mL of solution per gram of silica. The amount of tungsten salt dissolved was that necessary to obtain, after calcination, samples containing 0.5, 1, and 2 theoretical monolayers of WO_3, assuming that a "molecule" of WO_3 covers a surface of 17×10^4 pm^2 [17] and the specific surface area of the support, as determined by the BET method. The solvent was removed by evaporation in a water bath, and the solids thus obtained were dried at 373 K in air for 18 h, then manually ground in an agate mortar, and finally calcined in air for 3 h. Calcination temperatures ranged from 373 to 973 K. The samples are named as WS*X*/*T* (*X* standing for the number of theoretical monolayers of tungsta and *T* for the calcination temperature, in kelvin).

Crystalline WO_3, used as a reference, was synthesized by calcination of ammonium paratungstate at 723 K, while crystalline dodecatungstosilicic acid was commercial from Sigma.

Experimental Techniques. X-ray diffraction (XRD) profiles were recorded under ambient conditions in a Siemens D-500 instrument, using graphite-filtered Cu−Kα_1 radiation (λ = 154.05 pm) interfaced to a DACO-MP data acquisition microprocessor equipped with Diffract/AT software.

Nitrogen adsorption isotherms at 77 K, for surface area and porosity determination, were carried out in a conventional high-vacuum Pyrex system (residual pressure 10^{-4} N m^{-2}), pressure changes being monitored with an MKS pressure transducer. The samples were previously degassed in situ at 423 K for 2 h.

Raman spectra in the 200−1200 cm^{-1} range were recorded under ambient conditions on a computer-controlled Jobin Ybon spectrometer, model U-1000, using the 514.5 nm line from a Spectra Physics model 165 Ar^+ laser as the exciting source. The spectra shift width was typically 5 cm^{-1}, and laser source powers at the sample were ca. 400 mW.

S1089-5647(98)00614-2 CCC: $15.00
Published on Web 03/21/1998

X-ray absorption (XAS) data at the W−L_3 edge were collected at 77 K on wiggler station 9.2, at the Daresbury Synchrotron Radiation Source (UK), with an electron ring running at 2 GeV and 180−230 mA. Monochromatization was obtained with a double silicon crystal monochromator working at the (220) reflection, which was detunned 50% to reduce higher harmonics. Measurements were carried out in transmission mode using optimized ion chambers as detectors. Sample powders, diluted with boron nitride when necessary, were ground, homogenized, and pressed into self-supporting wafers, with total absorbance ca. 2.5 just above the W−L_3 absorption edge (10 202 eV) and edge jumps ≤1.0. At least three scans were recorded and averaged to obtain the experimental spectra. The EXAFS function $\chi(k)$ was obtained from the experimental XAS spectrum by conventional procedures.[18] Theoretical backscattering amplitude and phase shift functions for W−W and W−Si absorber−backscatterer pairs were calculated by using the program FEFF.[19a] Experimental functions for W−O absorber−backscatterer pairs were extracted from the spectrum of $Al_2(WO_4)_3$, a compound where W(VI) cations are surrounded[20] by four oxygen atoms at 1.78 ± 0.03 Å (forward Fourier transform: k^3-weighted, $\Delta k = 2.4-15.5$ Å^{-1}; inverse Fourier transform: $\Delta R = 0.6-2.2$ Å^{-1}). EXAFS data analysis and handling were performed by using the program package NEWEXAFS.[19b]

Temperature-programmed reduction (TPR) analysis was carried out on the samples, without any pretreatment, in a Micromeritics TPR/TPD 2900 instrument, at a heating rate of 10 K/min, using ca. 15 mg of sample and 60 mL min^{-1} of a H_2/Ar mixture as reducing agent (5 vol %, from Sociedad Española del Oxígeno, Valladolid, Spain). Experimental conditions for TPR runs were chosen according to data reported elsewhere[21] in order to reach good resolution of the component peaks.

FT-IR spectra of the samples were obtained with a Perkin-Elmer 16PC spectrometer, connected to an Ataio 386-SX computer, and using special cells with CaF_2 windows. Adsorption of pyridine, for surface acidity measurements, was also monitored by FT-IR spectroscopy. Samples were submitted to a conditioning treatment in situ, consisting of outgassing at 673 K for 2 h (residual pressure 10^{-3} N m^{-2}), previous to the adsorption studies.

Results and Discussion

Textural Properties. Nitrogen adsorption−desorption isotherms at 77 K on the parent support, and on selected samples, are shown in Figure 1. All isotherms are reversible in the pressure range studied and correspond to type II in the IUPAC classification,[22] characteristic of mesoporous solids. The specific surface area values determined following the BET method (S_{BET}) are given in Table 1. A steady decrease in S_{BET} is observed as the W content or the calcination temperature are increased. The behavior has been previously reported by Kerkhof et al.[23] and Thomas et al.[14] The cumulative surface area values and those determined from the *t*-plots are coincident (Table 1) with the S_{BET} values, as expected for mesoporous samples. Pore size distribution curves (Figure 2), show a major contribution by pores with an average diameter close to 3−4 nm for the support, without any noticeable change after loading tungsta.

Structure and Thermal Stability of Tungsten-Containing Phases. *X-ray diffraction* (XRD) diagrams for silica and tungsta-loaded samples calcined at 723 K are shown in Figure 3. The diagram for silica is typical for a mostly amorphous solid; on the contrary, diffraction diagrams for samples WS

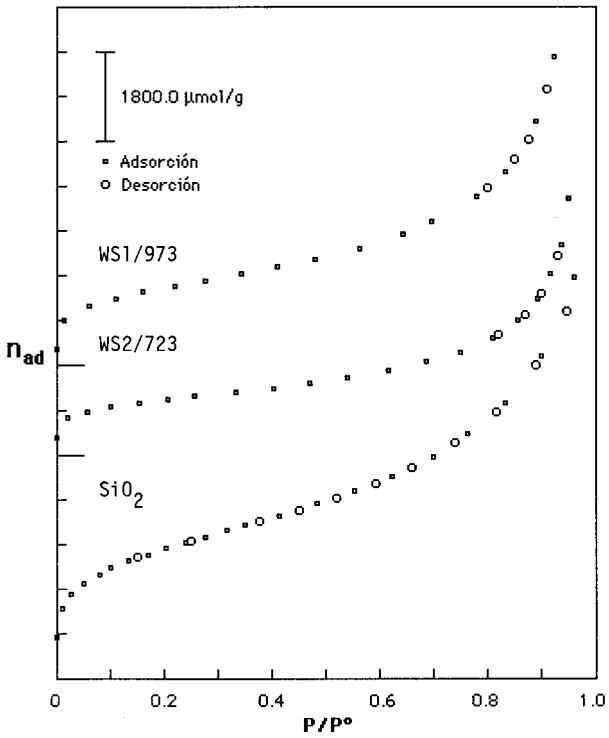

Figure 1. Nitrogen adsorption−desorption isotherms (77 K) on the support and on selected WS samples.

TABLE 1: Specific Surface Area Values[a] for the Support and the Tungsta−Silica Samples

sample	% W	S_{BET}	S_C	S_t
SiO_2		200	198	209
WS0.5/723	14.5	142	nm	nm
WS1/723	24.9	120	nm	nm
WS2/723	37.8	80	81	78
WS1/373	24.9	133	nm	nm
WS1/573	24.9	131	nm	nm
WS1/773	24.9	117	115	117
WS1/973	24.9	108	107	108

[a] In m^2 g^{-1}; nm = not measured.

calcined at 723 K show sharp diffraction lines, characteristic of crystalline species, with intensities that increase as the tungsten content does. However, the positions of these diffraction lines do not coincide with any crystalline species reported in the JCPDS files for compounds containing tungsten and oxygen (i.e., paratungstates, tungsta, H_2WO_4, etc.) or tungsten, silica, and oxygen. For some samples studied (WS0.5/723 and WS2/723), and in addition to the lines just described, weak lines corresponding to orthorhombic WO_3 (JCPDS file 20-1324) are also recorded. WO_3 lines could be due, at least for sample WS2/723, to tungsta in excess of the amount required to form the monolayer. It can also be formed upon thermal decomposition of the unknown species, as clearly observed in the XRD diagram of sample WS1/973 (Figure 3). In this case lines due to orthorhombic WO_3 appear with the simultaneous removal of diffraction lines observed in sample WS1/723, showing that the unknown species present in the sample calcined at 723 K is unstable at 973 K.

To assess the stability of this species, and the calcination temperature needed to form it, XRD diagrams of sample WS1 were recorded after calcining at temperatures ranging from 373 K (mere drying after impregnation) to 773 K (Figure 4). These still unassigned diffraction lines are already recorded after drying at 373 K, their intensities reaching maximum values after

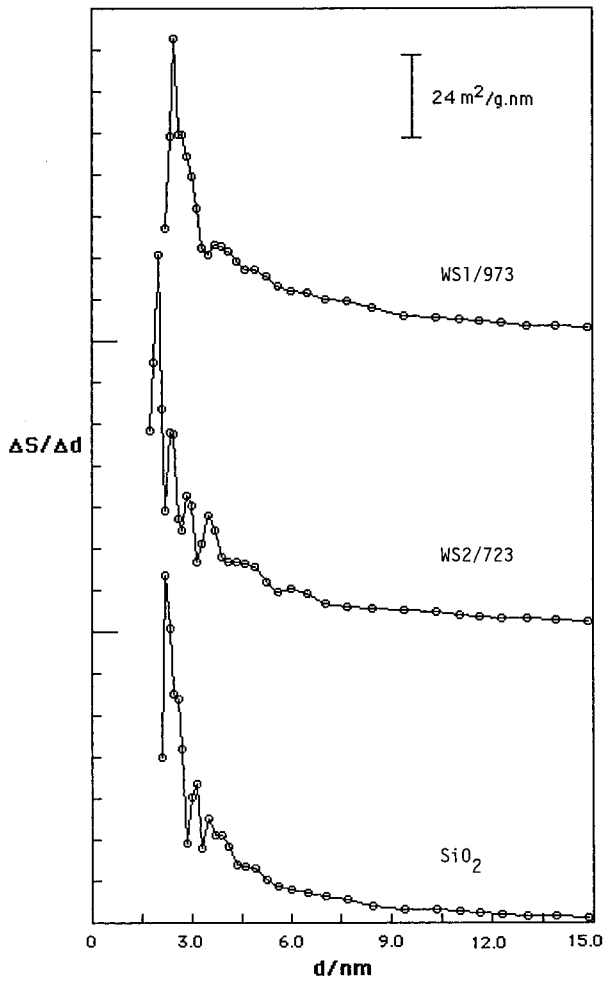

Figure 2. Pore size distribution curves for the support and selected WS samples.

calcination at 573−673 K. Decomposition to WO_3 takes place at 773 K, as at this temperature only diffraction peaks due to WO_3 are recorded. The diagram does not change markedly when the calcination temperature is further increased, only showing an increase in WO_3 crystallinity. A similar study has been carried out for sample WS0.5 (Figure 5). X-ray diffraction diagrams are very similar to those recorded for sample WS1, but in this case decomposition to WO_3 starts at a slightly lower temperature, 723 K. This fact indicates that when the W content is lowered, the stability of the unknown species decreases.

X-ray absorption spectra (XAS) at the W−L_3 absorption edge yield further information about the structure of tungsten-containing phases in WS samples. Experimental EXAFS oscillations for samples WS1 calcined at 573−873 K, and their associated Fourier transforms (FT), are included in Figure 6. In agreement with XRD results reported above, the FT of the spectrum recorded for WS1/873 (Figure 6d, solid lines) shows two distinct maxima at ca. 1.5 and 3.8 Å, which coincide with those recorded for crystalline, orthorhombic WO_3 (Figure 6d, dashed lines). This result confirms that after calcination at this temperature most of the tungsten cations are forming a WO_3-like phase on the surface of the silica support. Meanwhile, the local surrounding of tungsten cations in samples calcined up to 723 K is clearly different from that found in WO_3. FTs of EXAFS data for samples WS1/573 and WS1/723 (Figure 6, b and c) show significant changes both in the first coordination sphere (maxima at $R < 2$ Å) and in the second coordination sphere (maxima at 2.5−4 Å). The most distinct feature is a

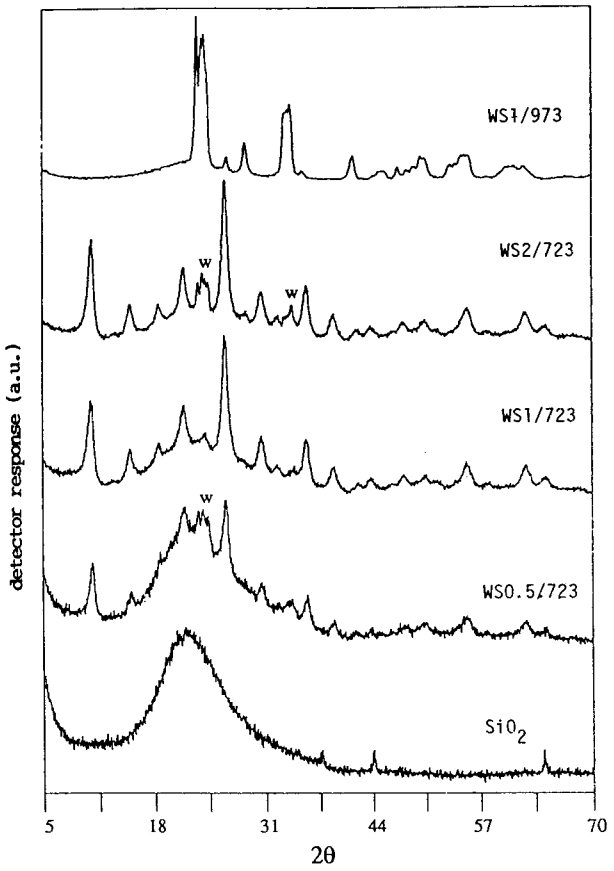

Figure 3. X-ray diffraction diagrams for the support and selected WS samples.

new, intense maximum at ca. 3 Å. Actually, EXAFS data for these samples are almost identical to that recorded for crystalline dodecatungstosilicic acid ($H_4SiW_{12}O_{40}{\cdot}nH_2O$, Figure 6b, dashed lines). This result shows that the short-range structure around tungsten in the unknown compound detected by XRD in WS samples is very similar to that present in dodecatungstosilicic acid.

Dodecatungstosilicic acid (hereafter SiW_{12}) is a type $H_{8-n}X^{n+1}M_{12}O_{40}$ heteropolyacid,[24] with $SiW_{12}O_{40}^{4-}$ anions that have the Keggin structure (Figure 7a) formed by 12 octahedra [WO_6] around and sharing corners with a central tetrahedron [XO_4]. The 12 octahedra [WO_6] are forming four clusters (each with three octahedra). Within each cluster, each octahedron shares two edges with neighboring octahedra. The clusters share corners to form the Keggin structure. This type of structure is formed with different X atoms (Si, B, P, ...) in the central tetrahedron and also in metatungstates, where the heteroatom at the center of the structure is substituted by two protons, thus forming $W_{12}O_{40}H_2^{6-}$ anions.[24] Tungsten cations are in a distorted octahedral coordination, with short W−O distances due to terminal W−O bonds, and longer W−O distances corresponding to W−O−W bridges and W−O−X bridges. At the second coordination shell, each tungsten cation has one heteroatom (X) and four W neighbors, two at 3.35 Å and two at 3.70 Å, associated respectively to edge-sharing and corner-sharing [WO_6] octahedra.

According to this structure, the simplest fit of W−L_3 EXAFS data for crystalline SiW_{12} (Figure 8, Table 2) is obtained within the single scattering (SS) approach by considering 5.5 oxygen atoms at the first coordination shell, distributed in two subshells at 1.72 and 1.92 Å, and a second coordination shell formed by 2.7 W atoms at 3.34 Å and 2.1 W atoms at 3.71 Å. These

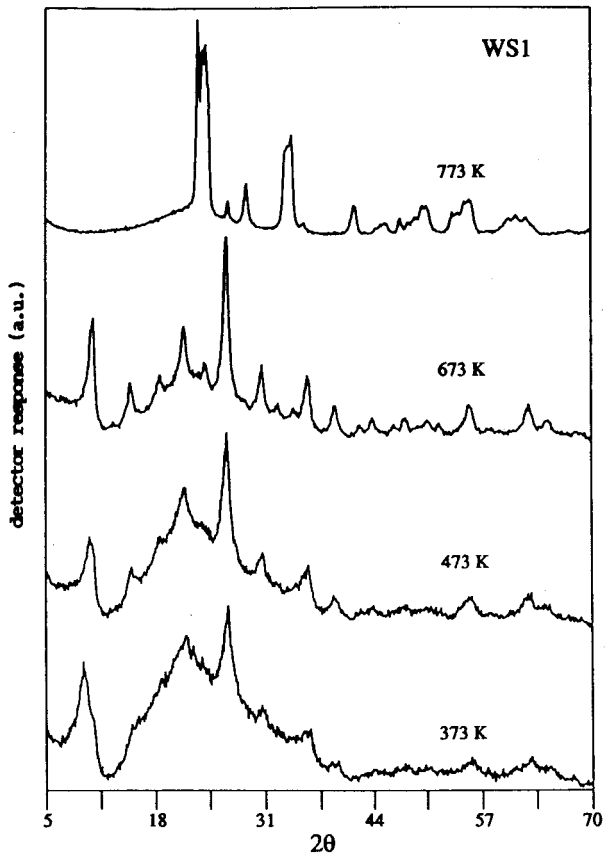

Figure 4. X-ray diffraction diagrams of sample WS1 calcined at the temperatures given (in K).

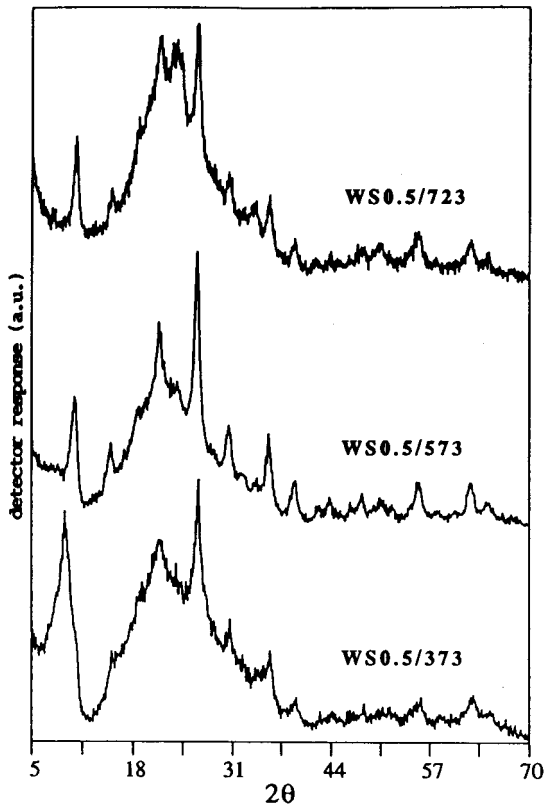

Figure 5. X-ray diffraction diagrams of sample WS0.5 calcined at the temperatures given (in K).

results agree with crystallographic data for barium dodecatungstosilicate dodecahydrate[25] and with the fit to the tungsten L_3-edge EXAFS of $[NBu_4^n]_3[PW_{12}O_{40}]$ recently reported by Evans et al.,[26] using a four-shell model including one terminal oxygen at 1.71 Å, four oxygens at 1.90 Å, two tungstens at 3.40 Å, and two tungstens at 3.68 Å. The quantitative relevance of multiple scattering (MS) effects contributing to the EXAFS

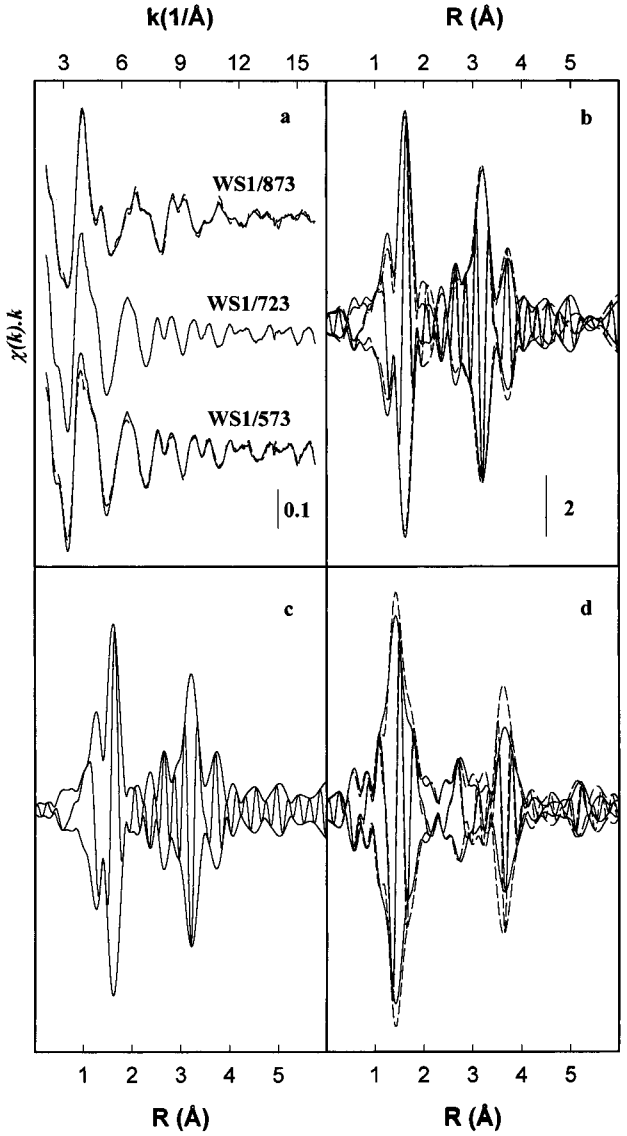

Figure 6. W−L_3 edge EXAFS data for WS1 samples (solid lines) and selected reference compounds (dashed lines). Experimental EXAFS oscillations for WS1 samples (a) and modulus and imaginary part of the associated k^3-weighted Fourier transforms for WS1/573 (b), WS1/723 (c), and WS1/873 (d). Data for hydrated $H_4SiW_{12}O_{40}$ and crystalline WO_3 have been superimposed to data for samples WS1/573 and WS1/873, respectively. ($\Delta k = 2.4-15.8$ Å^{-1} in all the Fourier transforms.)

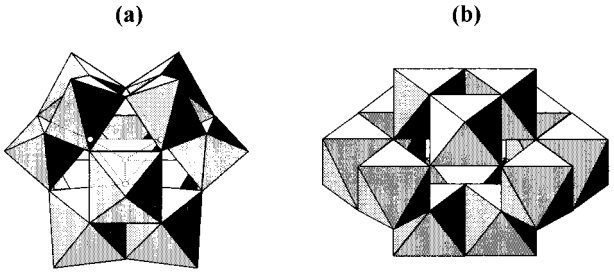

Figure 7. (a) Structure of the Keggin unit showing the central tetrahedral hole formed by inner oxygen atoms. (b) Structure of the paratungstate anion.

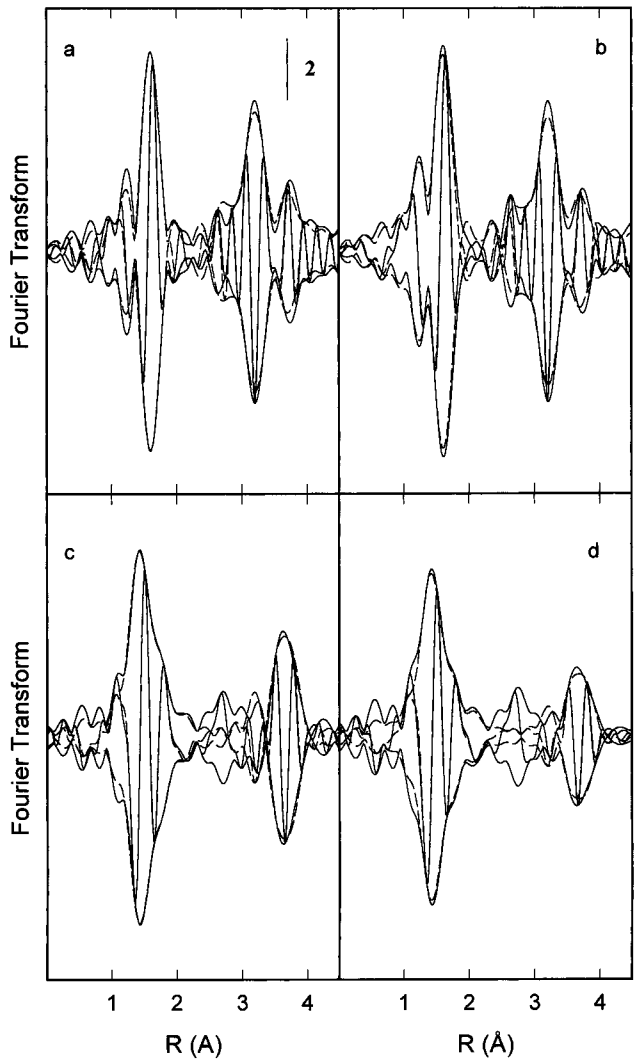

Figure 8. Best fit functions (dashed lines) to experimental W−L_3 EXAFS data (solid lines): (a) dodecatungstosilicic acid; (b) WS1/573; (c) orthorhombic WO_3; (c) WS1/873. k^3-weighted Fourier transforms. Fit ranges: $\Delta k = 3.0-15.5$ Å^{-1}; $\Delta R = 0-4.5$ Å.

signal can be accounted for by MS paths, discarded within the SS approach, was checked. A theoretical spectrum was calculated within a full MS approach using the FEFF code,[19a] and the cluster structure was generated from crystallographic data.[25] Main MS effects contributing to the EXAFS signal can account for MS paths arising from W−O−W bridges between vertex-sharing octahedra (bond angle 151 ± 6°). Other MS contributions, including those arising from W−O−W bridges between edge-sharing octahedra (bond angle 122 ± 5°), have a low relative intensity when working with a k^3-weighting scheme and within the analysis ranges here used ($\Delta k = 3-15.5$ Å^{-1}, $\Delta R = 0-4.5$ Å). Improvements in the quality of the fit to the experimental EXAFS spectrum, after the inclusion of the most intense MS path, were statistically unsignificant. The coordination number at the shortest W−W distance decreases from 2.7 Å, within the SS approach, to 2.1 Å after including this MS path, the latter value being closer to that expected for the Keggin structure. Meanwhile, values of shell radii are equal to those obtained in the SS approach within ±0.02 Å. Therefore, the SS approach accounts for the main features of the experimental spectrum, yielding reasonable coordination parameters.

Fit results within the SS approach for WS samples are also included in Figure 8 and Table 2. Coordination parameters for tungsten in WS1/573 are equal within the experimental error

TABLE 2: Best Fit Parameters for the W−L_3 EXAFS Spectra of Samples WS and Reference Compounds[a]

sample	atom	N	$\Delta\sigma^2$ (Å^2)	R (Å)	$\Delta E°$ (eV)
$W_{12}SiO_{40}^{4-}$	O	1.3	0.0005	1.72	−1.2
	O	4.2	0.0002	1.92	−0.1
	W	2.7	0.0026	3.34	1.5
	W	2.1	0.0031	3.71	−1.9
WS1/573	O	1.4	0.0000	1.74	0.1
	O	4.8	0.0010	1.92	−0.1
	W	2.5	0.0025	3.35	1.5
	W	2.1	0.0031	3.70	0.2
WS1/723	O	1.8	0.0003	1.74	0.1
	O	4.2	0.0002	1.92	−0.1
	W	2.0	0.0021	3.35	1.5
	W	2.1	0.0031	3.70	0.2
WS1/873	O	2.8	0.0000	1.79	1.4
	O	2.6	0.0058	2.12	−6.3
	W	3.4	0.0049	3.79	−1.5
	W	1.4	0.0041	3.87	−1.7
WO_3	O	2.8	−0.0007	1.79	1.4
	O	2.6	0.0035	2.12	−6.3
	W	5.6	0.0049	3.79	−0.9
	W	1.2	0.0045	3.87	0.9

[a] Estimated errors in coordination numbers (N) and shell radii (R) are ±15% and ±0.02 Å, respectively.

to that obtained for crystalline SiW_{12}. This result shows that the local order around tungsten cations, at both the first and second coordination shells, is identical to that found in Keggin-type units and, therefore, that most of the tungsten is forming this structure in the sample. Calcination at 723 K (sample WS1/723) produces a slight decrease of the W−W coordination number at the shortest distance, suggesting the decomposition at this temperature of a low fraction of Keggin units. It is worth noting that the intensities of diffraction lines associated with the unknown compound in WS1 samples reached their maximum values after calcination in the 573−673 K range and slightly decreased after calcination at 723 K.

Thomas et al.[6] detected small amounts of dodecatungstosilicic acid in W/SiO_2 samples prepared by wet impregnation, while Roosmalen et al.[27] considered the possible formation of silicon-bound tungstates, with a structure closely related to that of dodecatungstosilicates. More recently, Colque et al.[28] proposed that, in samples prepared by impregnation of silica with paratungstate solutions, an isopolytungstate is dispersed on top of the silica and transforms easily into bulk WO_3 when the sample is heated at 723 K. In our samples, EXAFS data show that tungsten forms a polytungstate with the Keggin structure that could be associated with either metatungstate or dodecatungstosilicate. The close coincidence between the number of short and long W−W distances determined for bulk SiW_{12} and WS samples discards in the latter a mere deposition of the paratungstate used during impregnation. As shown in Figure 7b, in the structure of paratungstate anions there are more [WO_6] units sharing vertex and fewer units sharing edges than in the Keggin structure.

Wachs et al.[29] have reported the formation of silicomolybdic acid (also with a Keggin-type structure) after exposing MoO_3/SiO_2 (prepared by impregnation of silica with heptamolybdate and calcination at 773 K) to water vapor at room temperature. Che et al.[30] have shown that MoO_3 and SiO_2 stirred in water for a period of time results in the formation of silicomolybdic acid. Formation of Keggin structures takes place under certain wet conditions.[30−32] In the present case, however, the heteropolyacid is formed during the dehydration process of the cake obtained after impregnation of silica with aqueous solutions of ammonium paratungstate; probably, the experimental condi-

tions used are similar to those reported by Wachs et al.[29] to be necessary to yield this acid.

To check whether silicon has entered in the Keggin unit as the central heteroatom, we have tested if W−L_3 EXAFS data are sensitive enough to detect the eventual presence of silicon at the second coordination shell of tungsten. A shell associated with the heteroatom was fitted by Evans et al.[26] to the W−L_3 EXAFS of $[PW_{12}O_{40}]^{3-}$, yielding a coordination number of 1.3 at 3.49 Å, and reported as statistically valid, since it had less than 1% probability of being insignificant. For bulk SiW_{12} the addition of a shell of 1.5 silicon atoms at 3.5 Å improves the quality of the fit, ϵ_ν^2,[33] from 47.4 to 35.7. Similar results were obtained when including a silicon shell (1.8 Si at 3.50 Å) in the fit to EXAFS data for WS1/573; ϵ_ν^2 decreases from 61.7 to 43.3. Unfortunately, in our case the probabilities for the silicon shell to be insignificant were higher than 4% and increased to 30% after including MS effects associated with W−O−W bridges. Therefore, EXAFS data do not allow to discriminate if Keggin units observed in WS samples are due either to the formation of SiW_{12} or to the crystallization of a metatungstate.

Increasing the calcination temperature of WS to 873 K (sample WS1/873) leads to a significant increase in the relative number of oxygen atoms at the shortest distance in the first coordination shell and a simultaneous lengthening of second-shell W−W distances, which now appear at 3.79 and 3.87 Å. Fit parameters for the latter sample in a single scattering approach are close to those obtained by fitting W L_3-edge EXAFS data for crystalline WO_3 (Table 2), where tungsten cations form distorted octahedral units, sharing edges in the three directions, thus leading to a tridimensional network.[24] Distortion of the $[WO_6]$ octahedra leads for the orthorhombic phase[34] to short (ca. 1.8−1.9 Å) and long (2.0−2.1 Å) W−O distances, accounted in the EXAFS fit by oxygen subshells at 1.79 and 2.12 Å, respectively, that yields a total coordination number in the first shell of 5.4, in excellent agreement with the expected value. At the second coordination shell, each tungsten cation is surrounded by six tungsten cations at 3.7−3.9 Å, corresponding to bridging W−O−W of corner-sharing octahedra. The best fit within the SS approach is achieved, in agreement with crystallographic data, with two W−W subshells at 3.79 and 3.87 Å and a total W−W coordination number of 6.8. As expected from a qualitative inspection of the spectra, fit parameters at the first coordination shell and W−W shell radii are identical, within experimental error, for both bulk WO_3 and WS1/873 (Table 2). W−W coordination numbers decrease by ca. 30% when going from bulk WO_3 to the supported sample, indicating some disorder in the supported tungsta phase. The quantitative relevance of MS paths in the W−L_3 EXAFS of WO_3 was also checked using a procedure identical to that reported above for SiW_{12}. Main MS contributions to the EXAFS can again account for MS effects arising from W−O−W bridges between the vertex-sharing octahedra that build this structure. Quasi-linear bridges in this structure (W−O−W angles between 168° and 180°) give rise to MS effects stronger than those found in the Keggin units (average W−O−W angles 151° and 122° respectively for vertex-sharing and edge-sharing octahedra). Other MS paths have a low relative importance, and they can be neglected when the analysis is performed with a k^3-weighting scheme. Improvements in the fit after the inclusion of the most intense MS path lead to a decrease in ϵ_ν^2 [33] from 75.1 to 58.2, although values obtained for W−W distances (3.78 and 3.88 Å) and the total W−W coordination number (6.2) do not change significantly from those obtained after fitting the spectrum on a single scattering scheme.

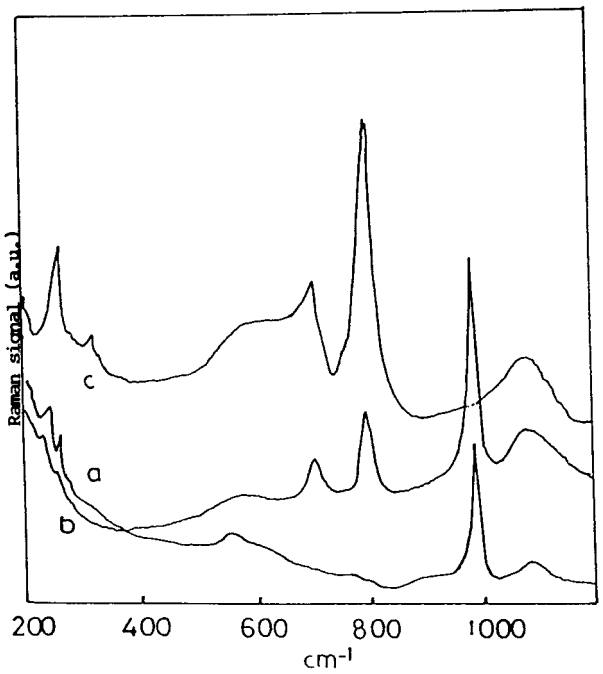

Figure 9. Raman spectra of samples WS1/723 (a), WS2/723 (b), and WS1/973 (c).

Raman spectra of selected WS samples are shown in Figure 9. For sample WS1/723 a sharp, intense band is recorded at 991 cm^{-1}. When the tungsten content is increased (sample WS2/723), new bands ascribed to crystalline WO_3[35] arise at 798, 711, and 266 cm^{-1}. Samples calcined above 773 K show Raman spectra (Figure 9, trace c) where the bands ascribed to crystalline WO_3 are clearly detected, while that at 991 cm^{-1} vanishes, allowing to ascribe it to Keggin-type units detected in samples calcined at low temperatures. Raman spectra reported[36] for $[SiW_{12}O_{40}]^{4-}$ and metatungstate anions exhibit intense bands at 998 and 977 cm^{-1}, respectively. The intense band recorded for WS samples at 991 cm^{-1} should be therefore ascribed to SiW_{12} units.

FT-IR spectra of samples WS1/723, WS1/773, and original, hydrated SiW_{12} are shown in Figure 10. Bands recorded for SiW_{12} (Table 3) coincide with that reported for this compound in ref 36, where an ascription of them is also given. The spectrum for sample WS1/723 shows, besides the broad band centered at 1125 cm^{-1} ascribed to the silica support, a weak absorption at 1400 cm^{-1}, indicative of the presence of ammonium cations, and other bands whose positions (980, 926, 882, 790, 540, and 476 cm^{-1}) coincide with those recorded for dodecatungstosilicic acid. The latter bands disappear after calcining at 773 K, giving rise to WO_3 bands. Table 3 also includes the main IR absorption bands for metatungstic acid and ammonium paratungstate (original and heated at 373 K), showing that significant changes are expected between IR spectra of these isopolyanions and that of SiW_{12}. Therefore, IR results definitely discard the formation of para- or metatungstate structures in WS samples and indicate that silicon has effectively entered the Keggin units formed after calcining at moderate temperatures. It is worth noting that XRD data show that this compound is already detected when the samples were merely dried after impregnating the silica support with the paratungstate solution. Therefore, there is a total reaction between the tungstate solution and the silica support during the own impregnation step. Moffat et al.[37] previously reported that Keggin-type compounds were formed when silica was impregnated with molybdate solutions. In our case, and taking into

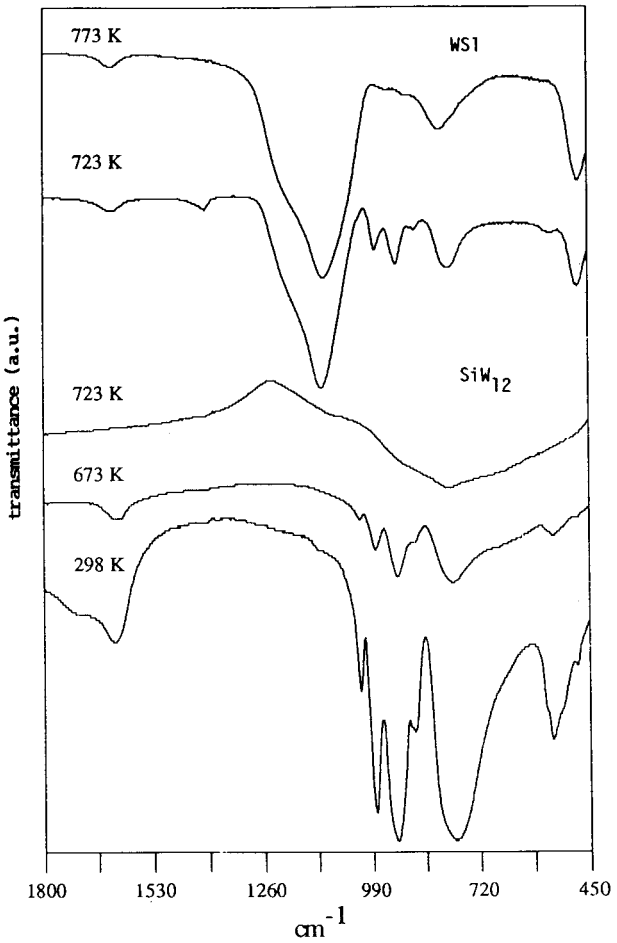

Figure 10. FT-IR spectra of dodecatungstosilicic acid and sample WS1 calcined at the temperatures given (in K).

TABLE 3: Position (cm^{-1}) of the Main Infrared Bands for Selected Polytungstates[a]

compound	position
dodecatungstosilicic acid[b]	1019 (m), 980 (s), 926 (s), 883 (m), 787 (s, b), 540 (m) 476 (m)
ammonium paratungstate[b]	1402 (s), 932 (m), 868 (m), 819 (w), 702 (s, b), 613 (w, sh) 532 (m), 496 (m)
ammonium paratungstate calcined at 373 K[b]	1402 (s), 967 (sh), 883 (m), 790 (s, b)
metatungstic acid[c]	960 (m), 935 (s), 870 (s), 770 (s)

[a] s = strong; m = medium; w = weak; b = broad; sh = shoulder. [b] This work. [c] From ref 36.

account tungsten loading and support specific surface area, there is a Keggin unit by 176 $Å^2$ in WS1/723. This value is within the range of cross sections reported for Keggin units in the approximation of close packing of anions (144 $Å^2$ in ref 38, 200 $Å^2$ in ref 39). In fact, Keggin units are covering the support surface, since there is a strong decrease in the intensity of infrared bands ascribed to OH groups over the silica surface (band centered at 3432 cm^{-1}) when going from the bare support to the WS1/723 sample.

Thermal stability of this compound seems to depend on the tungsten loading. This parameter is of interest since low thermal stability of heteropolytungstates limits their use as a heterogeneous catalyst. Figure 10 includes FT-IR spectra recorded after calcining the commercial SiW_{12} compound at increasing temperatures. As shown by these spectra, the characteristic bands of the Keggin-type unit have completely disappeared after calcining bulk dodecatungstosilicic acid at 723 K, indicating

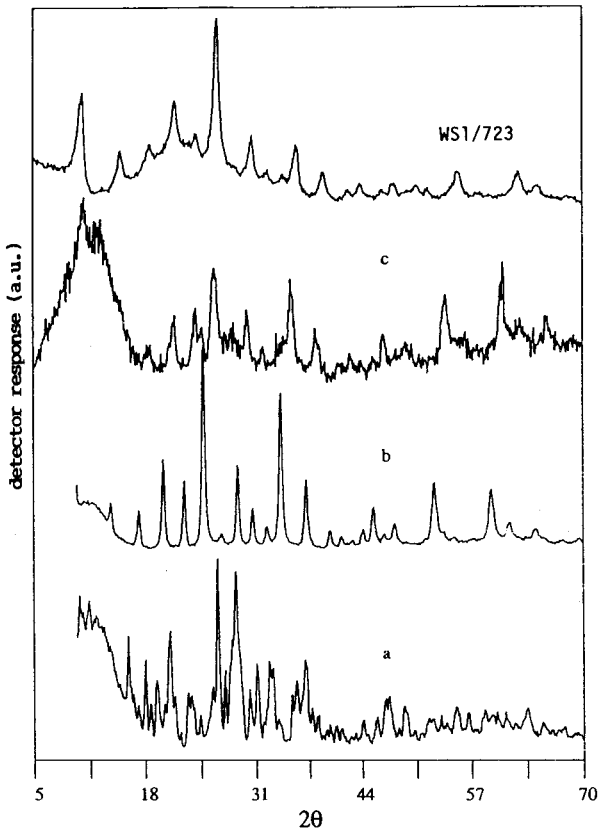

Figure 11. X-ray diffraction diagrams of dodecatungstosilicic acid calcined in air at 293 (a), 573 (b), and 673 K (c). The diagram for sample WS1/723 is also shown.

that thermal decomposition has been achieved at this temperature. It should be stressed that results reported above show that most of the SiW_{12} units formed in WS samples are stable after calcining at 723 K, showing some stabilization of this species. We want also to note that, although spectroscopic data undoubtedly show that in WS samples calcined at moderate temperatures tungsten is forming a compound with Keggin-type units identical to those found in commercial dodecatungstosilicic acid, diffraction lines for both compounds do not match. This difference could be due to the presence of ammonium cations, detected in FT-IR spectra of WS samples by a band at 1400 cm^{-1}, and to a different hydration degree in both compounds, since XRD diagrams of these compounds were reported to depend on the hydration degree.[40] To check further this possibility, we have monitored the evolution of the XRD diagram of SiW_{12} calcined at different temperatures, up to its total transformation to WO_3. As shown in Figure 11, the XRD diagram for bulk SiW_{12} changes as the calcination temperature is increased, and although none exactly matches with those recorded for samples WS, there are strong similarities between the WS diagram and the most intense lines for dodecatungstosilicic acid calcined at 673 K. The lack of total agreement may be due to a different packing of the Keggin units in the partially dehydrated acid and in WS samples, due to the presence of ammonium cations and/or to their interaction with the silica surface in the latter case.

Reducibility and Surface Acidity of Tungsten−Silica Samples. *Temperature-programmed reduction* (TPR) profiles of reference samples, bulk WO_3 and SiW_{12}, and several WS samples are included in Figure 12. The bare support (not shown) does not show any reduction in the temperature range here studied.

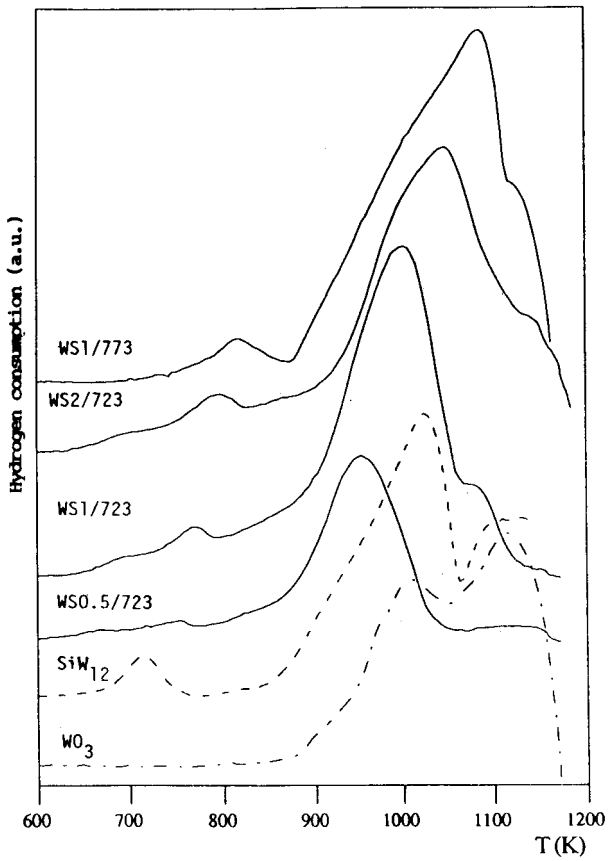

Figure 12. Temperature-programmed reduction profiles for crystalline WO_3, dodecatungstosilicic acid, and selected WS samples.

As expected, the shape and position of the main reduction maxima for bulk dodecatungstosilicic acid coincide with data for crystalline WO_3, since the reference SiW_{12} sample decomposes to WO_3 at temperatures lower than the onset of this reduction process. Besides this main reduction band, a weak reduction process is recorded for bulk tungstosilicic acid at 715 K, which may be tentatively ascribed to a partial reduction of W^{6+} species in the Keggin units.

Reduction profiles for samples WS0.5/723, WS1/723, WS2/723, and WS1/773 also show a weak reduction maximum between 715 and 815 K and a broad reduction maximum between 952 and 1088 K. Both maxima shift toward higher temperatures as the tungsten content or the calcination temperature is increased. Previous data in this paper show that in the 800−900 K temperature range, where the main reduction process starts, surface Si−O−W species are completely decomposed to WO_3, and this process should have been completed during the steady heating in the TPR run previously to the onset of the reduction process at 900−1200 K. However, it should be noted that the main reduction maxima recorded for WS samples are different from those obtained for crystalline WO_3, suggesting for WS0.5/723 and WS1/723 a single step reduction of WO_3 formed from Si−O−W species present in the original sample. This reduction is easier than from bulk WO_3, as shown by a significant decrease in the temperature of the maximum. Reducibility is also higher than for tungsten oxide supported on alumina or magnesia.[17,41] Hydrogen consumption in the full temperature range studied is summarized in Table 4, where the percentage of WO_3 reduction has been calculated assuming reduction from W^{6+} to W^0. A complete reduction is observed for sample WS1/773, the reduction degree decreasing for samples calcined at 723 K. Among samples calcined at 723 K, the highest reduction degree is achieved for the WS1 sample.

TABLE 4: Summary of Temperature-Programmed Reduction Data for Samples WS

sample	T^a	R−WO_3[b]	sample	T^a	R−WO_3[b]
SiW_{12}	1023	nm	WS2/723	1048	67
WS0.5/723	952	72	WS1/773	1088	100
WS1/723	1000	89			

[a] Position (K) of the main reduction maximum. [b] Weight percentage of WO_3 reduction. SiW_{12} = dodecatungstosilicic acid; nm = not measured.

TABLE 5: Position (cm^{-1}) and Ascription of the Main FT-IR Bands Recorded after Adsorption of Pyridine

	Bpy[a]			Lpy[b]			
sample	8a	19a	19b	8a	8b	19a	19b
SiO_2				1596[c]			1447[c]
WS0.5/723	1638	1488	1538	1614 1597[c]		1488	1445
WS1/723	1638	1487	1536	1613 1597[c] (sh)	1577	1487	1451
WS2/723	1636	1487	1538	1610 1597[c]	1577	1487	1447
WS1/773				1615 1609 (sh) 1597	1576	1490	1446

[a] Protonated pyridine bonded to surface Brönsted acid sites. [b] Pyridine coordinated to surface Lewis acid sites. [c] Physisorbed pyridine. sh = shoulder.

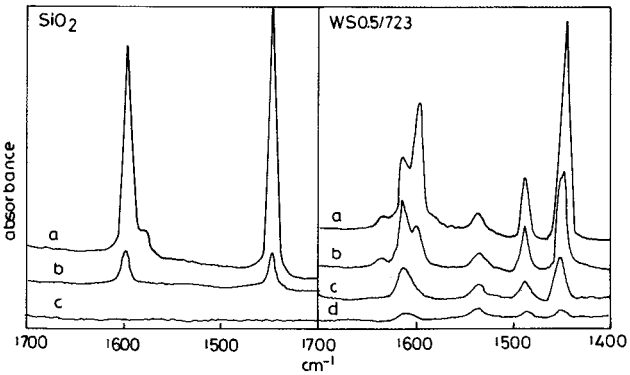

Figure 13. FT-IR recorded after adsorption of pyridine at room temperature on SiO_2 and sample WS0.5/723 and outgassed at (a) room temperature, (b) 373 K, (c) 473 K, and (d) 573 K.

FT-IR Monitoring of Pyridine Adsorption. In agreement with results reported by other authors,[42,43] the FT-IR spectrum recorded after adsorption of pyridine at room temperature on the bare support shows bands at 1596 and 1447 cm^{-1}, ascribed to modes 8a and 19b of physisorbed pyridine (Table 5 and Figure 13), which almost vanish after outgassing at 473 K. In addition to bands at 1596 and 1447 cm^{-1}, the spectrum recorded for sample WS0.5/723 (Figure 13) shows bands at 1614 and 1488 cm^{-1}, due to coordination of pyridine to surface Lewis acid sites (Table 5). Weaker bands are recorded at 1638 and 1538 cm^{-1}, due to modes 8a and 19b of protonated pyridine, indicating that the presence of tungsten-containing species leads to development of surface Brönsted acid sites. Intensities of all these bands decrease after outgassing at increasing temperatures, but they are still recorded even after outgassing at 573 K, showing that both types of acid sites are rather strong.

Similar spectra are recorded for samples WS1/723 and WS2/723 (Figure 14), but bands due to coordinated and protonated pyridine are stronger while the bands due to physisorbed

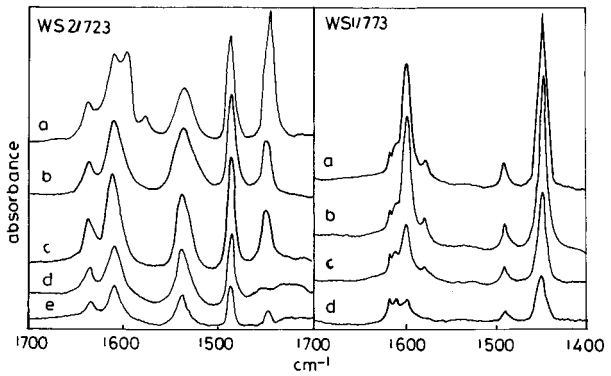

Figure 14. FT-IR recorded after adsorption of pyridine at room temperature on samples WS2/723 and WS1/773 and outgassed at (a) room temperature, (b) 373 K, (c) 473 K, and (d) 573 K.

pyridine are weaker than in WS0.5/723. Outgassing at increasing temperatures leads to a decrease in the intensities of the bands, although those ascribed to Lewis and Brönsted acid sites are recorded even after outgassing at 673 K, thus definitively showing that surface acid sites are strong.

On the contrary, the spectrum recorded for sample WS1/773 shows the most intense bands in the same positions as for adsorption on bare silica (1597 and 1446 cm^{-1}). Weak bands at 1615, 1609, and 1490 cm^{-1} are recorded even after outgassing at 573 K and correspond to coordination of pyridine molecules to two types of surface Lewis acid sites, as the band due to mode 8a splits. The component at 1615 cm^{-1} coincides with the band recorded for samples calcined at lower temperatures, while the component recorded at 1609 cm^{-1} is probably related to the presence of crystalline WO_3, the most abundant species in this sample. The characteristic bands of the pyridinium ion are absent, thus showing that surface Brönsted acid sites do not exist in this sample. The behavior of bands at 1597 and 1446 cm^{-1} should be noted. For WS1/773 they are still recorded after outgassing at 573 K, while for the bare support they almost vanished after outgassing at 473 K, thus suggesting that in WS1/773 they do not correspond to physisorbed pyridine but to coordination to weak surface Lewis acid sites.

Surface acid sites in metal oxides should be usually related to their electronegativity; however, silica (an oxide of a rather electronegative element, such as silicon) does not show surface Lewis acid sites, due to the lack of coordinatively unsaturated cations on its surface. A similar behavior is observed for vanadia, molybdena, or tungsta, where surface concentration of Lewis acid sites is rather low, despite the electronegativities of the corresponding elements being similar to those of aluminum or titanium, whereas alumina and titania develop surface Lewis acid sites due to their particular surface structure and coordinative insaturation of surface cations. Development of strong surface Lewis acid sites on silica after supporting other transition-metal cations such as Fe, Mo, Cr, etc., has been reported previously.[44,45]

In our samples, development of strong surface Lewis acid sites is related to the presence of coordinatively unsaturated W^{6+} species in the Keggin-type units formed upon interaction between the paratungstate solution and silica or in supported WO_3 formed by thermal decomposition of these Keggin units. Surface Brönsted acid sites, also existing in samples calcined at 723 K, are related to the presence of Keggin-type units, as bridging Si−O−W or terminal W−O bonds are easily protonated, leading to formation of bridging or terminal hydroxyl groups.[44] Although a quantitative analysis of surface concentration of Brönsted or Lewis acid sites has not been carried out, reported data allow to conclude that when the tungsten content is raised, the surface concentration of these sites increases, due to an increase in surface concentration of complex species covering (*carpeting*) the silica surface, thus accounting for a decreased physisorption on the bare support surface.

The different types of surface Lewis acid sites detected in the sample calcined at 773 K can be assigned as follows: (i) coordinatively unsaturated W^{6+} ions in Keggin-type units (band at 1613 cm^{-1}), probably still existing in a dispersed form, and (ii) coordinatively unsaturated W^{6+} species in WO_3 (band at 1609 cm^{-1}), as WO_3 is the major component of this sample. These two types of surface Lewis acid sites should be rather strong, although their concentration should not be too large, as the bands are weak. A third type of surface Lewis acid sites, giving rise to the strongest bands at lower wavenumbers that coincide with those recorded on silica, could be related to Si^{4+} species. Although these species are coordinatively saturated in bare silica, transformation of surface tungstosilicate to WO_3 in this sample calcined at 773 K leads to formation of anion vacants at the surface, thus giving rise to coordinatively unsaturated Si^{4+} species, now acting as Lewis acid sites.

Conclusions

The results here obtained show that both variables studied (i.e., tungsten concentration and calcination temperature) modify the nature of the supported species and therefore the physicochemical properties of these systems. For calcination temperatures up to 723 K, silica is covered by Si−O−W species, forming Keggin-type units similar to those found in dodecatungstosilicic acid. The thermal stability of this species depends on tungsten concentration, and it is stable up to 723 K for tungsten loadings equivalent or higher than that corresponding to a theoretical monolayer of WO_3 over the support surface. Orthorhombic WO_3 is formed upon thermal decomposition of the samples. All these species are more easily reduced than tungsta/alumina or tungsta/magnesia samples. Surface acidity of samples calcined up to 723 K is very large, developing both Brönsted and Lewis acid sites associated with the dodecatungstosilicate species; on the contrary, only surface Lewis acid sites are detected in samples calcined at higher temperatures, where only WO_3 is detected.

Acknowledgment. Financial support from DGICYT (grant PB93-0633) is acknowledged. We thank Daresbury Laboratory (UK) for allocating beam time for XAS measurements (Grant 25/359). G. Solana acknowledges a sabbatical leave from Universidad de Guanajuato (México).

References and Notes

(1) Salvati, L.; Makovsky, L. E.; Stencel, J. M.; Brown, F. R.; Hercules, D. M. *J. Phys. Chem.* **1981**, *85*, 3700.
(2) Horsley, J. A.; Wachs, I. E.; Brown, J. M.; Via, G. H.; Hardcastle, F. D. *J. Phys. Chem.* **1987**, *91*, 4014.
(3) Hilbrig, F.; Göbel, H. E.; Knözinger, H.; Schmelz, H.; Lengeler, B. *J. Chem. Phys.* **1991**, *95*, 6973.
(4) Vuurman, M. A.; Wachs, I. E. *J. Phys. Chem.* **1992**, *96*, 5008.
(5) Kohler, S. D.; Ekerdt, J. G.; Kim, D. S.; Wachs I. E. *Catal. Lett.* **1992**, *11*, 227.
(6) Thomas, R.; Moulijn, J. A.; de Beer, V. H. J.; Medema, J. *J. Mol. Catal.* **1980**, *8*, 161.
(7) Thomas, R.; Moulijn, J. A. *J. Mol. Catal.* **1980**, *8*, 161.
(8) Banks, R. L. *Fotsch. Chem. Forschung.* **1972**, *25*, 39.
(9) Mol, J. C.; Moulijn, J. A. *J. Mol. Catal.* **1982**, *15*, 157.
(10) Haines, R. J.; Leigh, G. J. *Chem. Soc. Rev.* **1975**, *4*, 155.
(11) Van Roosmalen, A. J.; Mol, J. C. *J. Catal.* **1982**, *78*, 17.
(12) Luckner, R. C.; Wills, G. B. *J. Catal.* **1973**, *28*, 83.
(13) Thomas, R.; Van Oers, E. M.; De Beer, V. H. J.; Medema, J.; Moulijn, J. A. *J. Catal.* **1982**, *76*, 241.

(14) Thomas, R.; Van Oers, E. M.; De Beer, V. H. J.; Moulijn, J. A. *J. Catal.* **1983**, *84*, 275.
(15) Kim, D. S.; Ostromecki, M.; Wachs, I. E.; Kohler, S. D.; Ekerdt, J. G. *Catal. Lett.* **1995**, *33*, 209.
(16) Misono, M. In New Frontiers in Catalysis; *Proceedings of the 10th International Congress on Catalysis*; Guczi, L., Solymosi, F., Tétény, P., Eds.; Elsevier: Amsterdam, 1993; p 69.
(17) Vermaire, C.; Van Berge, P. C. *J. Catal.* **1988**, *116*, 33.
(18) Sayers, D. E.; Bunker, B. A. In *X-ray Absorption: Principles and Applications of EXAFS, SEXAFS and XANES*; Königsberger, D. C., Prins, R., Eds.; Wiley: New York, 1988.
(19) (a) Rehr, J. J.; Zabinsky, S. I.; Albers, R. C. *Phys. Rev. Lett.* **1992**, *69*, 3397. (b) Rehr, J. J. *Jpn. J. Appl. Phys.* **1993**, *32*, 8.
(20) De Boer, J. J. *Acta Crystallogr. B* **1974**, *30*, 1878.
(21) Malet, P.; Caballero, A. *J. Chem. Soc., Faraday Trans. 1* **1988**, *84*, 2369.
(22) Sing, K. S. W.; Everett, D. H.; Haul, R. A. W.; Moscou, L.; Pierotti, L. A.; Rouquerol, J.; Sieminiewska, T. *Pure Appl. Chem.* **1985**, *57*, 603.
(23) Kerkhof, F. P. J. M.; Moulijn, J. A.; Thomas, R.; Odejans, J. C. *Stud. Surf. Sci. Catal.* **1979**, *3*, 77.
(24) Wells, A. F. *Structural Inorganic Chemistry*, 5th ed.; Oxford University Press: Oxford, 1987.
(25) Kobayashi, A.; Sasaki, Y. *Bull. Chem. Soc. Jpn.* **1975**, *48*, 885.
(26) Evans, J.; Pillinger, M.; Rummey, J. M. *J. Chem. Soc., Dalton Trans.* **1996**, 2951.
(27) Van Roosmalen, A. J.; Koster, D.; Mol, J. C. *J. Phys. Chem.* **1980**, *84*, 3075.
(28) Colque, S.; Payen, E.; Grange, P. *J. Mater. Chem.* **1994**, *4*, 1343.
(29) Bañares, M. A.; Hu, H.; Wachs, I. E. *J. Catal.* **1995**, *155*, 249.
(30) Rocchiccioli-Deltcheff, C.; Amirouche, M.; Che, M.; Tatibouët, J. M.; Fournier, M. *J. Catal.* **1990**, *125*, 292.
(31) Misono, M. *Catal. Rev.—Sci. Eng.* **1987**, *29*, 269; **1988**, *30*, 339.
(32) Ogata, A.; Kazusaka, A.; Yamazaki, A.; Enyo, M. in *Acid−Base Catalysis*; Tanabe, K., Hattori, H., Yamaguchi, T., Tanaka, T., Eds.; VCH: Weinheim, 1989; p 249.
(33) ϵ_ν^2 values were calculated as described by Lytle et al. (Lytle, F. W.; Sayers, D. E.; Stern, E. A. *Physica B* **1989**, *158*, 701).

$$\epsilon_\nu^2 = \frac{\nu}{N_p(\nu - N_f)} \sum_{i=1}^{N_p} \frac{[\chi_{\mathrm{model},i} - \chi_{\mathrm{exp},i}]^2}{\sigma^2}$$

N_p = number of experimental data; N_f = number of free parameters; $\nu = 2\Delta k.\Delta R/\pi + 1$; σ = mean error in experimental data, taken as 10^{-3}.

(34) Salje, E. *Acta Crystallogr. B* **1977**, *33*, 574.
(35) Beattie, I. R.; Gilson, T. R. *J. Chem. Soc. A* **1969**, 2322.
(36) Rocchiccioli-Deltcheff, C.; Thouvenot, R.; Franck, R. *Spectrochim. Acta A* **1976**, *32*, 587.
(37) Kasztelan, S.; Payen, E.; Moffat, J. B. *J. Catal.* **1988**, *112*, 320.
(38) Brückman, K.; Haber, J.; Lalik, E.; Serwicka, E. M. *Catal. Lett.* **1988**, *1*, 35.
(39) Rocchiccioli-Deltcheff, C.; Amirouche, M.; Herbé, G.; Fournier, M.; Che, M.; Tatibouët, J. M. *J. Catal.* **1990**, *126*, 591.
(40) Hodnett, B. K.; Moffat, J. B. *J. Catal.* **1994**, *88*, 253.
(41) Martín, C.; Rives, V.; Solana, G.; Malet, P. *J. Catal.* **1997**, *169*, 516.
(42) Parry, E. P. *J. Catal.* **1963**, *2*, 371.
(43) Rajadhyaksha, R. A.; Knözinger, H. *Appl. Catal.* **1989**, *51*, 81.
(44) Kataoka, T.; Dumesic, J. A. *J. Catal.* **1988**, *112*, 66.
(45) Martín, C.; Mendizábal, M. C.; Rives, V. *J. Mater. Sci.* **1992**, *27*, 5575.